# ENHANCED PROBLEM SOLVING; THE INTEGRATION OF CFD AND OTHER ENGINEERING APPLICATIONS

**Ross HAYWOOD[1*], Wes TAYLOR[1], Tom PLIKAS[2], Nathan TEDFORD[2], and Dave WARNICA[2]**

[1] Hatch, 61 Petrie Terrace, Brisbane Australia

[2] Hatch, 2800 Speakman Drive, Mississauga, Canada

*Corresponding author, E-mail address: rhaywood@hatch.com.au

## ABSTRACT

Two case studies are presented in which Computational Fluid Dynamics (CFD) has been used in conjunction with other models to solve real engineering problems. The first combines CFD with Finite Element Analysis (FEA) for stress analysis and examines the failure and re-design of the central pipe (vortex finder) in an alumina gas suspension cyclone. The second problem requires the interfacing of a CFD solution of gas-phase flow, combustion and heat transfer within a rotary kiln with a simplified 1-D heat and mass balance model that simulates the complex coupled thermal-chemical processes occurring in the bed. In both cases the detailed understanding of the fluid flow and thermal transport provided by CFD expands the capabilities of the secondary models and has yielded reliable engineering solutions for complex mechanical and process problems.

## INTRODUCTION

CFD has a well established track-record as an advanced modelling tool providing significant benefit across a range of engineering applications in the metals and energy industries. CFD has become widely used (and in some cases part of the standard methodology) for the engineering of ventilation and emission capture systems, reactor design, off-gas handling systems, and water cooled equipment among others. Recent developments in the aerospace industry have driven the development of modelling tools that can feasibly address problems which feature a coupled flow and mechanical stress analysis – Flow Structure Interaction (FSI). However, in the chemical and process industries the kinds of problems that are more likely to be coupled to the fluid flow would be thermal stress analysis, or detailed process chemistry and thermodynamics. Examples of these types of problems and the coupling of CFD to related modelling tools are the focus of this investigation.

## I) VORTEX FINDER

After cracks were found between the gussets and shell on the main support ring of vortex-finders within both preheat and calcination cyclones in a major alumina production facility, Hatch was engaged to investigate a new vortex-finder design. The rapid development of an improved design was essential to prevent a possible catastrophic failure of the existing units and to take advantage of an approaching window of opportunity afforded by an upcoming planned maintenance outage to implement the required modifications.

### Nature of the problem

Figure 1 below shows the CAD solid model of the vortex-finder, gusset plates and support ring for the cyclone (typical). A photo and sketch of the vortex-finder are shown in Figures 2 and 3 respectively. The photo illustrates the nature of the observed problem with failure of the connection between the gussets and main shell and plastic deformation of the vortex-finder shell below the refractory packing. The sketch provides details of the gusset/ support ring/ cyclone-body mechanical configuration.
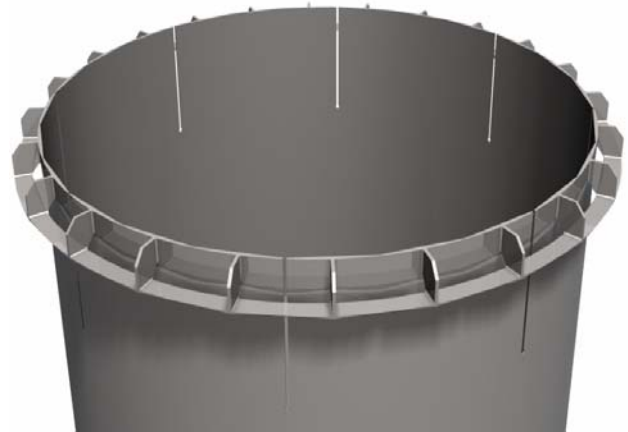


**Figure 1.** CAD rendering of existing vortex-finder showing support ring linked to body by gussets.
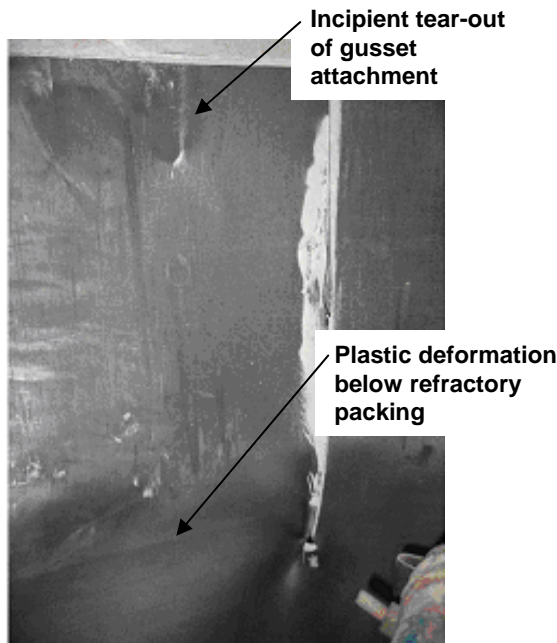
**Figure 2.** Photo of existing Vortex-finder showing regions of plastic deformation
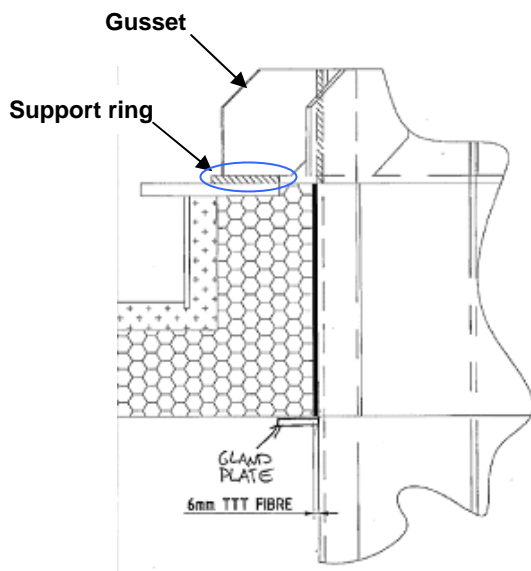


**Figure 3.** Sketch showing gusset and support ring detail with refractory packing.

Computation of the resulting thermally induced stress and deformation of the vortex finder under steady operating conditions was straight forward and the equivalent stress when the system is isothermal at $600^0$C is shown in Figure 4. Due to symmetry the solution is only required over a segment of the complete system. Peak stresses were predicted to occur in the main body of the vortex finder at the gusset connection and at the lowest point in the expansion slots. Significant deformation was predicted to occur just below the refractory packing. The FEA model clearly predicts the observed behaviour.
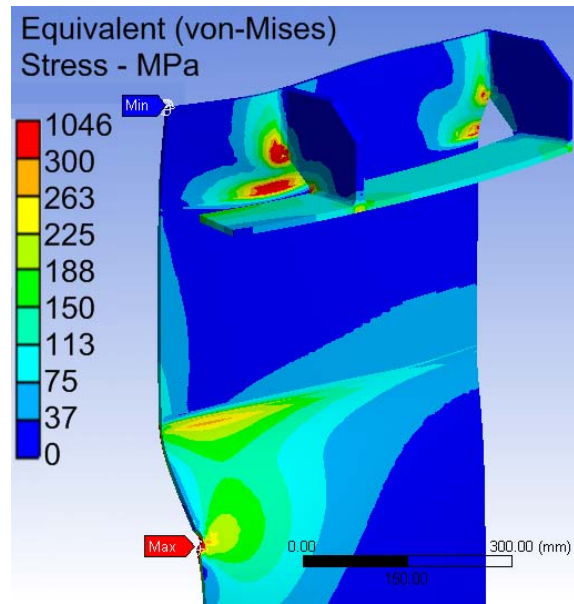


**Figure 4** – Stress at $600^0$C rigid packing material assumed

A number of possible modifications to the original design were investigated to reduce the stress and deformation to acceptable levels. The preliminary solution was simply to increase the number of expansion slots around the circumference of the vortex finder.

While the provision of additional expansion slots was considered a practical solution to the difficulties arising from thermal stresses in the vortex-finder during steady operation, there was some concern that frequent thermal transients in the bulk gas-phase flow (related to sudden loss or commencement of solids feed) could be contributing to the observed problems. Figure 5 shows the typical system behaviour during these transient periods. A transient thermal stress analysis was deemed necessary.
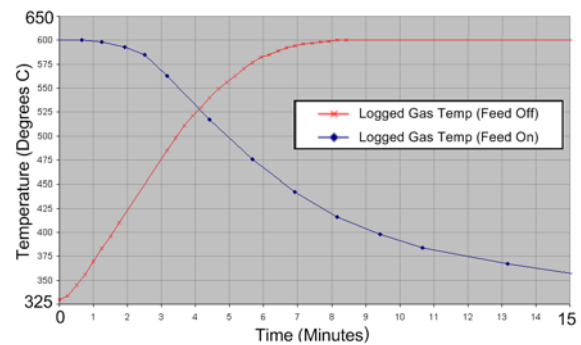


**Figure 5.** Transient gas temperature plot from instrumentation system.

Consideration of transient thermal conditions (feed-on/feed-off scenarios) and their effects on the vortex-finder required an understanding of the convection heat transfer within the system. A computational fluid dynamic (CFD) model was developed to simulate the flow and heat transfer within the preheating Cyclone. This then formed the basis for the thermal conditions to be used in the FEA.

## Results

Computations of the fluid flow and heat transfer showed the heat transfer coefficient at the vortex-finder external surface to be reasonably uniform with a maximum near the cyclone inlet, where the inlet flow impinges on the vortex-finder outer surface, and an adjacent minimum in the region above where the flow has spiralled downwards leaving a zone of low velocity. On the internal surface of the vortex-finder the heat transfer is less uniform due to the strong swirl of the gas-phase and the entrance effect as the flow enters the vortex-finder. Regions of low heat transfer coefficient are seen in the wake of each of the expansion slots. The average heat transfer coefficients on the external and internal surfaces of the vortex-finder are 101, and 134 $W/m^2K$, respectively. Results are shown in Figures 6 and 7.

A transient CFD analysis including conjugate heat transfer in the solid vortex finder was performed to examine the peak temperature differences circumferentially. The results showed that the biggest variation in temperature around the vortex-finder body was in the order of only $10^{O}C$. This was not expected to cause any stress or deformation related problems, and therefore was not investigated any further.
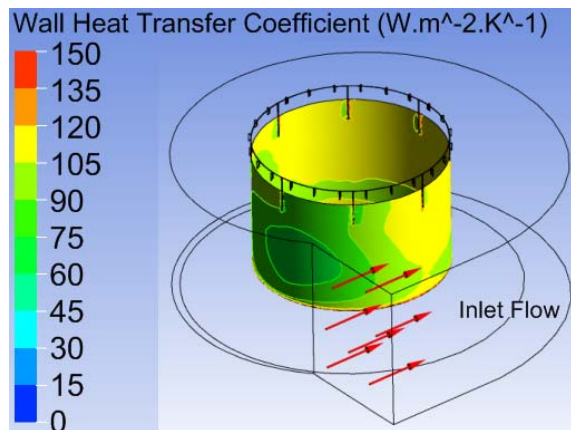


**Figure 6.** CFD results showing the heat transfer coefficient on the outer surface of the vortex finder
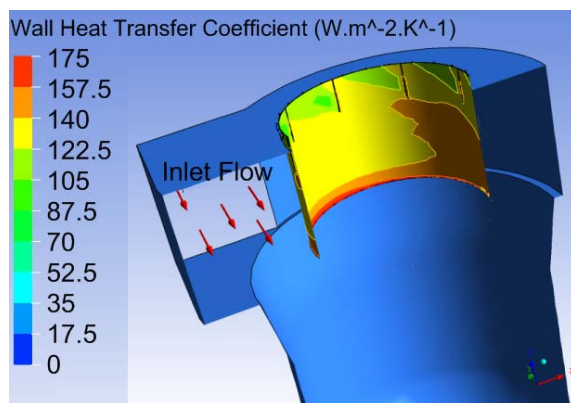


**Figure 7.** CFD results showing the heat transfer coefficient on the inner surface of the vortex finder

Computations of the transient FEA were based on the heat transfer coefficients derived from the CFD analysis (Figures 6 and 7), and a prescribed transient variation in the bulk gas temperature, as seen in Figure 5. The heat transfer coefficients and the transient bulk-gas temperature history were manually input. Future software releases are reported to be incorporating automated transfer of volumetric temperature data which would have significantly streamlined this process.

Typical results are shown in Figures 8 (steady thermal conditions) and Figure 9 (transient conditions in which the gas-phase temperature is decreasing ie., a feed-on scenario).
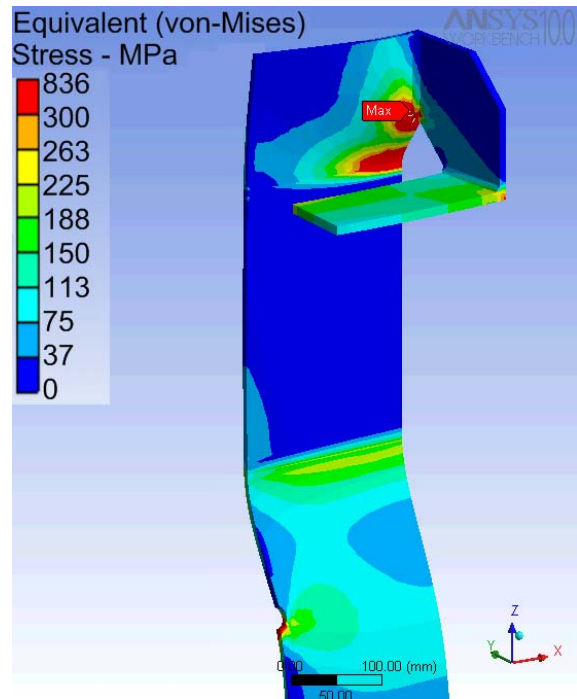


**Figure 8** - Stress at $900^{0}C$ proposed modification using additional expansion slots.
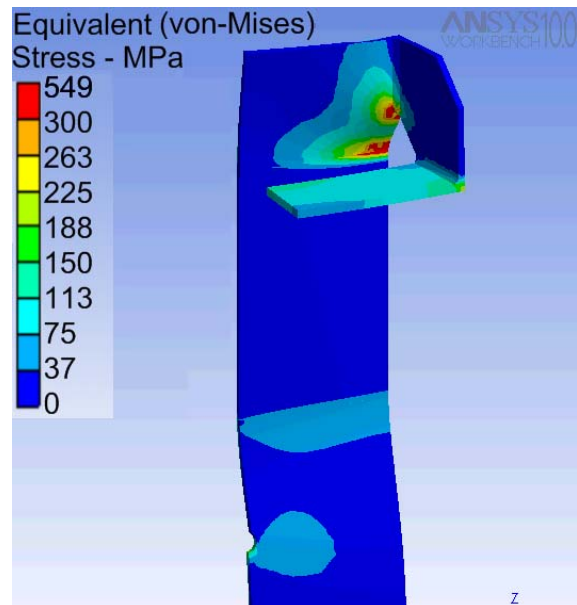


**Figure 9 -** Transient Stress 34 minutes after Feed On - proposed modification

The results can be summarised as follows:

- the support ring temperature lags the gas temperature by many hours. It takes ~28 hours for the ring to reach the full gas temperature (ignoring conduction of heat through the refractory to the support ring)
- the "feed on" transient causes the body to heat up before the support ring forcing it to push radially on the gussets and force them apart. Conversely, the "feed off " transient causes the body to cool down before the support ring, forcing it to pull radially on the gussets and force them together.
- the combination of the feed on and off transients causes fatigue failure of the gusset connections.
- The "feed off" transient produces the lowest stress magnitudes of all load cases ("feed on" and static were similar)
- The expansion slots do not completely solve the radial growth issue. This was resolved by modifying the refractory design and allowing greater radial expansion allowance on the main body, to prevent the gussets trying to pull the body through solid refractory.
- The redesigned vortex-finder is subjected to lower stresses than the original in virtually all operating scenarios

While it was not possible to automate fully the coupling of CFD and FEA solutions in this instance, it should be possible in a future release of ANSYS-CFX. Direct linkage of the CFD derived temperature field into the FEA analysis will be a priority when the next opportunity arises.

## II) ORE ROASTING KILN

As one of the primary process vessels in the metallurgical industry, rotary kilns are used in numerous applications including calcination, drying, reduction, and roasting of ores and concentrates. Combustion in the gaseous zone of the kiln provides the energy required for the phase transformations and chemical reactions to occur in the solids bed. The combustion, or process, gases typically flow counter-current to the flow of solids in the bed. Heat transfer can be enhanced through the use of internal devices such as chains, dams, and lifters. Process gas flow over the bed also results in dust generation and elutriation of particles from the kiln.

Given the complex multi-physics and multi-phase mechanisms occurring in the kiln, a full analysis of the process performance using a single, standard analytical tool is difficult. To this end, Hatch has developed a methodology whereby a CFD model of the gaseous zone is integrated with a one-dimensional mass and energy balance model of the solids zone to predict the process performance in the kiln. The two distinct models are coupled to predict accurately the heat and mass exchange between the gaseous and solids zones.

This modelling approach allows for robust, reliable, and efficient characterization of kiln process performance. Design modifications are quickly and efficiently analysed using this tool to determine technical viability, and make recommendations for detailed engineering of process and equipment.

### One-Dimensional (1D) Kiln Model

This is a proprietary model developed by Hatch written in the Fortran programming environment. It is an adaptation of the kiln model by Venkateswaran & Brimacombe (1977) based on a 1D, finite volume representation of the governing equations for mass and energy conservation. All solid and gas properties are averaged over the kiln cross-section at each axial control volume location making the model one dimensional in the axial direction. Although this model does include a Gibbs free energy minimization routine for the prediction of gaseous conditions at thermodynamic equilibrium, the CFD model is used instead to predict the gas conditions because its ability to simulate more accurately the combustion phenomena occurring here. The CFD model also more accurately predicts the radiation network exchange occurring in the gaseous zone of the kiln.

The strength of the 1D kiln model is in its ability to simulate the complex phase changes and chemical reactions occurring in the solids bed. Moisture removal kinetics and thermodynamics can be included, as well as rate expressions for calcination, reduction, de-sulphidation, and roasting reactions. Considerable flexibility exists in the model to modify reaction chemistry as well as physical and thermodynamic properties of the various chemical components present, making the model adaptable to different types of rotary kiln and dryer operations. The model also includes expressions to predict the increased heat transfer from the gas to the solids as a result of chains, dams, and material lifters.

### CFD Model

The CFD model calculates the detailed gas flow, mixing, combustion, and heat transfer in the gaseous zone of the kiln. Burners are included and the combustion is modelled assuming the reactions are either mixing rate or kinetically limited, or that partial or full thermodynamic equilibrium is achieved. The particular assumption used depends on the type of process occurring, fuel type, fuel-air ratios, and temperatures inside the kiln.

The CFD model includes a simplified geometric representation of the solids bed for heat and mass exchange. The information pertaining to bed performance is determined from the 1D kiln model, and applied as a boundary condition at the bed surface in the CFD model. The CFD model predicts the heat transfer (by radiation and convection) to this boundary condition, as well as any mass transfer. This information is then passed back to the 1D kiln model for re-calculation of the bed surface condition. This process is repeated until a steady-state converged solution is achieved.

### Application to Iron Ore Concentrate Drying and Roasting in Kiln

Hatch has recently applied this methodology to evaluate and optimize the performance of a rotary kiln used for processing of iron ore concentrates in a large metallurgical facility. In this particular application, a rotary kiln 4 m in diameter and 110 m long, was installed for the purposes of removing free and bound moisture from the ore concentrate, followed by roasting of the ore to meet the product quality requirements.

The kiln was unable to meet these requirements, particularly with regards to roasting. The kiln could not achieve a residence time of 30 minutes at or above 920°C required for roasting of the ore at the design throughput.

A study was performed to determine the technical feasibility of achieving the desired residence time in the kiln by modifying the combustion equipment, the kiln internals, and the operating conditions.

### Existing Process Performance in Kiln

The first step in the analysis was to simulate the existing kiln operation to ensure the models are representative of process performance. The models were run for a specific operating condition where measurement data was available for validation purposes.

The primary reactions in the solids bed involve the removal of free and bound moisture, which occur from 100°C to 320°C. Proper roasting of the ore requires a solids temperature at or above 920°C. A natural gas burner is located at the ore discharge end of the kiln that provides the heat for these processes. The 1D kiln model was adapted to include these processes and their specific rate expressions and thermodynamic properties.

A CFD model of the kiln was constructed in Gambit and ANSYS Fluent to simulate the gas phase combustion and heat transfer. The model geometry is shown in Figure 10, and includes the internal gaseous volume of the kiln, the refractory shell of the kiln, the surface of the ore bed, and the duct arrangement for secondary and tertiary air. A separate CFD model was built for the natural gas burner which includes all internal passages for fuel and primary air flow, swirl vanes, and holes for fuel discharge. The flow conditions at the outlet of the burner model were set as inlet conditions for the kiln model. For both models, a hybrid grid consisting of hexahedral, prismatic, and tetrahedral cells was used to mesh the fluid and solid volumes. Grid adaption was done in ANSYS Fluent to refine the grid for improved accuracy in the prediction of reaction rates and flame profiles.

Combustion was modelled using the Eddy-Dissipation model of Magnussen and B. H. Hjertager (1976), except that the mixing rate constants A and B were modified for improved prediction of the reaction extent based on Hatch experience. Radiation was modelled using the Discrete Ordinates model, and turbulence modelled using the Realizable k-e model.

Figure 11 shows the average gas and solids temperature predicted by the CFD and kiln model, respectively. As mentioned previously, coupling between the two models was performed to arrive at this solution. The solids temperature at the discharge end of the kiln was measured for this specific operating condition, and the model prediction compares favourably with the data. Table 1 shows a comparison of the outer shell temperature of the kiln, with good agreement between the model and data attained.
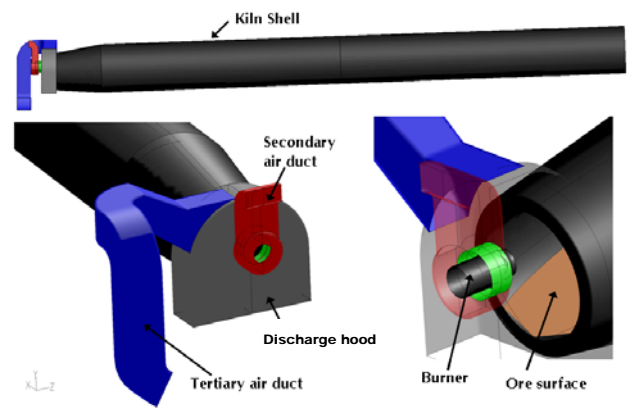


**Figure 10.** Geometry for CFD model.

The modelling exercise indicates that the poor performance of the kiln (negligible residence time at or above 920°C) is caused by a deficit of energy from the gaseous zone, and by short flame lengths (8-10 m), which cannot provide the radiation heat transfer to the ore required to raise the temperature to the desired target for roasting. The kiln had been operating at a reduced throughput as a result.

| Location | Measured | CFD prediction |
| --- | --- | --- |
| 8 m downstream of burner | 310°C | 290°C |
| 12 m downstream of burner | 290°C | 277°C |
| 30 m downstream of burner | 212°C | 202°C |

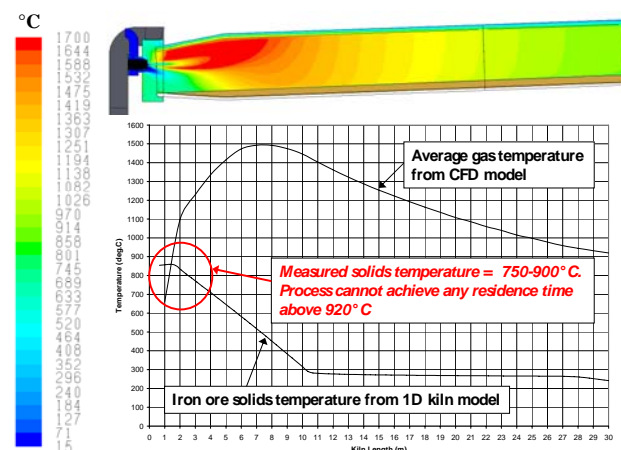**Table 1.** Measured versus Predicted Outer Shell Temperatures of Kiln.



**Figure 11.** Gas and solids temperature in kiln predicted by CFD and kiln model, respectively, for existing kiln operation. The measured solids temperature is also shown for comparison.

### Predicted Process Performance in Kiln after Modifications

Several options were considered to improve process performance, and the modelling was instrumental in evaluating and assessing the technical feasibility of each option in a quick and efficient manner. These included: changing burner settings, modification of secondary & tertiary air delivery systems, use of dams and material lifters, preheating of ore concentrate, and utilization of on-board fans. The final recommended solution involved preheating of the ore concentrate upstream of the kiln to reduce specific energy requirements in the kiln, and staging the combustion process in the kiln to reach and maintain the desired ore temperature for roasting. Figure 12 shows the predicted process performance with these modifications incorporated.

A substantial improvement over the existing kiln performance is realized, as the roasting temperature of 920°C is maintained for greater than 30 minutes. Staging the combustion is accomplished through the use of on-board fans, which are mounted on the external shell of the kiln and rotate with the kiln. The fans force ambient air into the centre of the kiln through heat resistant pipes. An illustration of an on-board fan arrangement is shown in Figure 13. The quantity of air injected is controlled to achieve the desired natural gas combustion at each stage. By necessity, the primary, secondary, and tertiary air flows at the burner are reduced to create sub-stoichiometric (rich) conditions at this end of the kiln. It was determined that a new burner was not required, and the exiting burner could be utilized in combination with the on-board fan arrangement.
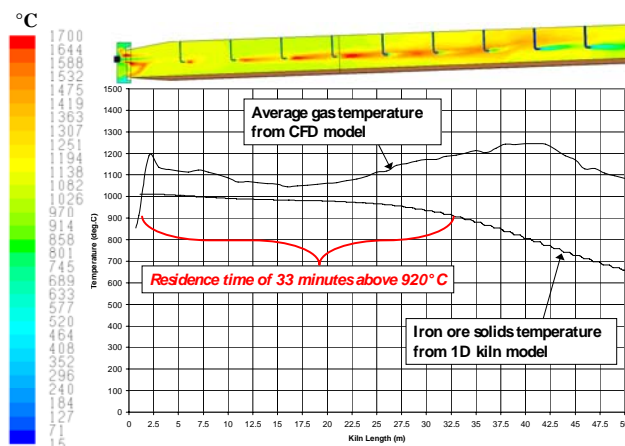


**Figure 12.** Gas and solids temperature in kiln predicted by CFD and kiln model, respectively, for modified combustion system configuration.
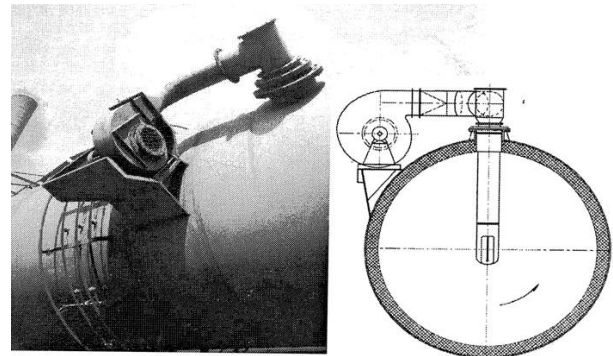


**Figure 13.** Fan mounted on external shell of kiln. Fan rotates with the kiln. From: Kashani-Nejad et. al. (2005).

## CONCLUSION

Combining CFD with other engineering models that provide solutions for thermal stress analysis and detailed process chemistry has been shown to extend the range of application of CFD in the minerals and process industries and provide solutions to challenging and multi-faceted industrial problems.

## REFERENCES

KASHANI-NEJAD, S., et. al., (2005), "Modelling of nickel laterite kiln processing – A conceptual review", *Nickel and Cobalt 2005 Challenges in Extraction and Production, 44th Annual Conference of Metallurgists of CIM*, Calgary, Canada.

MAGNUSSEN, B.F. and HJERTAGER, B. H. (1976), "On mathematical models of turbulent combustion with special emphasis on soot formation and combustion", *16th Symp. (Int'l.) on Combustion*. The Combustion Institute.

VENKATESWARAN and BRIMACOMBE, (1977), "Mathematical model of the SL/RN Direct Reduction Process", *Met Trans B*, Vol. 8b, pp. 387-398